Reaction-induced microcracking: An experimental investigation of a mechanism for enhancing anatectic melt extraction

J. A. D. Connolly* Institute for Mineralogy and Petrography, Swiss Federal Institute of Technology, Zurich 8092, Switzerland
M. B. Holness Department of Geology and Geophysics, University of Edinburgh, West Mains Road, Edinburgh EH9 3JW, United Kingdom
D. C. Rubie Bayerisches Geoinstitut, Bayreuth University, Bayreuth D-95440, Germany
T. Rushmer Department of Geology, University of Vermont, Burlington, Vermont 05405

ABSTRACT

Melting reactions can create melt overpressure that may induce microcracking. To determine whether such microcracking can enhance rock permeability and melt extraction, we have studied the partial melting of a muscovite-bearing metaquartzite at 800 MPa and 950–1126 K. Melting begins at muscovite-quartz grain boundaries and results in progressive replacement of muscovite by melt pools containing mullite and biotite. The volume change for the reaction (0.021 m^3 per m^3 of original rock) generates randomly oriented microcracks that emanate from melting sites. The mean crack length in two-dimensional sections is 151 ± 5 μm and reflects the spacing between melting sites. Experiments in which quartz sand was loaded with the metaquartzite to act as a drain verified that the microcracks, together with the melt pools, form a connected network. The estimated network permeability is $10^{-14\pm1}$ m^2, at least four orders of magnitude greater than permeabilities characteristic of regional metamorphic environments. For reaction-induced microcracking to occur, the reaction must take place on a time scale such that creep cannot accommodate the associated volume change. Our analysis suggests that that requirement can be met on regional metamorphic time scales and that reaction-induced microcracking is a feasible mechanism of permeability enhancement during partial melting and devolatilization.

INTRODUCTION

Experimental and theoretical models have shown that in texturally equilibrated rock-melt systems the permeability of the rock matrix is too low to permit efficient anatectic melt extraction (e.g., McKenzie, 1985; Laporte and Watson, 1995). The constraint on permeability arises from the expectation that in texturally equilibrated systems, granitic melt occupies either isolated pores or a porosity connected by tubelike channels (e.g., Wolf and Wyllie, 1991; Laporte and Watson, 1995). Recognition of this limitation has led to the suggestion that externally induced deformation perturbs the equilibrium melt distribution so as to enhance the matrix permeability and facilitate melt extraction (e.g., Miller et al., 1988; Rutter and Neumann, 1995). An alternative cause of deformation is the volume change associated with the melting reaction itself. The volume change of many crustal melting reactions is positive and thus a potential cause of embrittlement (e.g., Clemens and Mawer, 1992; Petford, 1995). If cracks generated by reaction-induced embrittlement form a connected network, then melt extraction will be facilitated without, or in tandem with, external deformation. Here we report results of an experimental investigation to assess the feasibility of reaction-induced embrittlement as a mechanism for enhancing melt extraction. The motivation for this work came from an earlier study of melting kinetics in a muscovite-bearing metaquartzite (Brearley and Rubie, 1990). In this earlier study, melt-filled cracks were observed that appeared to have propagated from melted muscovite grains. The most probable explanation for this observation is that the cracks originated because of melt overpressure. We have done additional experiments to establish this relationship unambiguously, and to determine whether the microcracks form a connected (i.e., permeable) network.

*E-mail: jamie@erdw.ethz.ch.

EXPERIMENTAL AND ANALYTIC METHODS

The starting material is a strongly foliated, but otherwise homogeneous muscovite-bearing metaquartzite consisting of 90.7 ± 3.3 vol% quartz and 9.3 vol% muscovite, with trace quantities (<0.1 vol%) of zircon and chlorite (for chemical analyses see Brearley and Rubie, 1990). The foliation (Figs. 1A and 2A) is formed by muscovite grains, 0.24 ± 0.2 mm across and 0.042 ± 0.02 mm thick (reported errors are a 95% confidence interval on the mean, grain sizes are the average of >100 measurements with no stereological correction). Quartz occurs as equant grains 0.09 ± 0.02 mm in diameter. The experimental charges were 4.8-mm-diameter cores, 6–10 mm long. The cores were dried at 343 K and sealed in platinum capsules with flat end-pieces. The capsules were partially submersed in water to minimize heating during welding. In some runs, a 2–3-mm-thick layer of clean, sorted (0.125–0.150 mm), beach (quartz) sand was added on one end of the charge to provide a drain for the melt (Rutter and Neumann, 1995). The experiments were done in internally heated Ar-pressurized vessels at 1123–1193 K and 790–820 MPa (Table 1). To bring the samples to experimental conditions, pressure and temperature were raised simultaneously. At experimental conditions, temperature and pressure were controlled within ±5 K and ±1 MPa. The runs were isobarically quenched to subsolidus temperatures in about 20 s, and to room temperature within 2–3 min. The rapid quenches caused extensive microfracturing of the charges, but cracks formed in this manner are not melt filled.

After each run, the charges were sectioned parallel and orthogonal to the foliation, mounted in epoxy, chemically polished, and coated with a 1.5-pm-thick layer of carbon for electron microscopy. The most successful imaging technique for identifying the melt-filled cracks was backscattered-electron microscopy (7.5 nA beam current, 15 kV accelerating voltage, and 20 mm working distance). In the resulting images, melt-filled cracks can be distinguished from grain boundaries and quench cracks because the melt phase (glass) has a higher average atomic number than the quartz matrix and is therefore brighter. In this paper, we consider only the melt-filled cracks. One to three images were made of each sample for image analysis; each image was of a 4.6 mm^2 area with a resolution 0.8 pixel per 1 μm. Threshold and "white top-hat" filters (Serra, 1988) were used to isolate the cracks in each image. Each crack was characterized by the length and orientation of a chord drawn between the crack endpoints.

EXPERIMENTAL RESULTS

The melting reaction observed in all samples is similar to the metastable melting reaction in the water-saturated experiments described by Brearley and Rubie (1990). The reaction begins along muscovite-quartz grain contacts and results in the progressive replacement of muscovite and surrounding quartz by a melt pool containing mullite and biotite (Fig. 1A). This reaction occurs in natural environments characterized by high melting (heating) rates (e.g., Grapes, 1986; Moecher et al., 1996) and is metastable with respect to the reaction muscovite + quartz = melt + sanidine + sillimanite (± biotite), which would be the equilibrium reaction at roughly 750 K at 80 MPa (Storre, 1972). The average atomic proportions of the major nonvolatile cations in the melt are

$$K_{0.0691}Na_{0.0274}Fe_{0.0047}Mg_{0.0097}Si_{0.7213}Al_{0.1678}$$

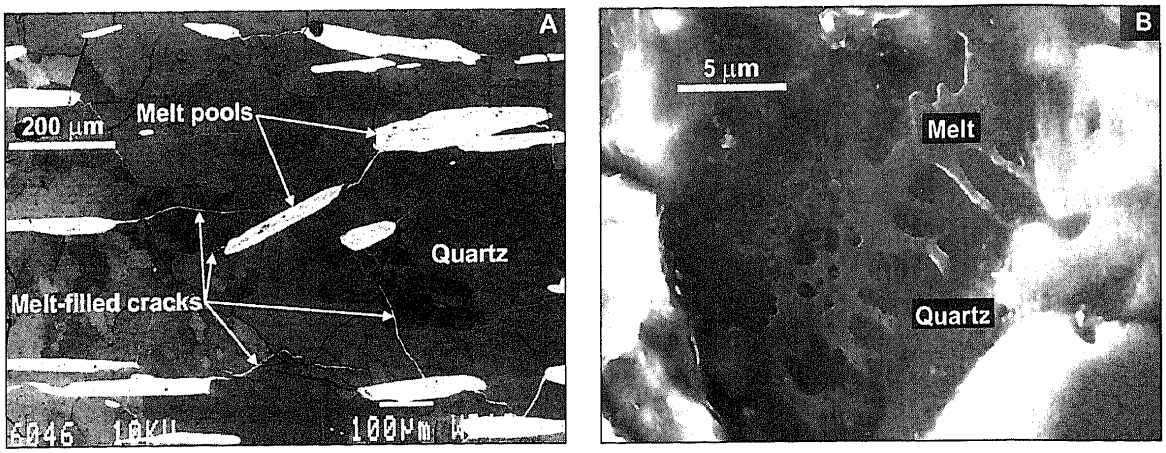

Figure 1. Scanning backscattered-electron microscopy images (orthogonal to foliation plane) from experiment U7 (Table 1). A: Cracks and melt pools after incongruent muscovite + quartz melting. Bright elongate regions are melt pools partially filled by mullite, biotite, and relict muscovite. B: Melt along crack surface, texture indicates that cracks are partially healed (U7, Table 1).

TABLE 1. EXPERIMENTAL CONDITIONS AND RESULTS

Run	P (MPa)	T (K)	t (h)	Rxn (%)	Qtz (%)	$\bar{c}'$ (μm)	n	d (m^{-1})
U3a	790	1193	116	100	87	119 ± 6	162	4177
U3b	790	1193	116	100	90	135 ± 7	126	3702
					94	195 ± 16	87	3690
U5	820	1193	14	100	79	115 ± 8	49	1224
U6	820	1193	24	100	83	110 ± 6	82	1967
U7	830	1193	3	87	90	104 ± 6	131	2948
					76	170 ± 12	86	3182
U8	820	1193	1	88	85	104 ± 6	81	1836
					88	187 ± 24	49	1996
D600.1	780	1193	24	100	87	84 ± 11	16	302
D600.2	780	1193	24	100	—	154 ± 14	64	2149
D600.3	780	1193	24	100	87	155 ± 12	97	3267
D602	790	1193	119	100	—	124 ± 8	96	2594
D604	780	1193	115	100	82	131 ± 9	81	2302
D605	820	1123	6	28	82	121 ± 7	75	1966
					76	183 ± 14	48	1908
D606	820	1123	2	38	89	148 ± 11	57	1834
					88	187 ± 25	33	1345

Note: Runs prefaced by D and U indicate, respectively, drained and undrained experiments. Rxn is volume percentage of melt + reaction products within melt pools, Qtz is total volume percentage quartz, $\bar{c}'$ is mean crack length ($\pm 2\hat{\sigma}_m$), n is number of observations per sample (area = 4.6 mm^2), and d is total crack length per 1 m^2. Where two sets of results are listed for a single run, first set is from foliation-orthogonal section, and second set is from foliation-plane section. In run D605, draining was orthogonal to foliation; in all other drained runs draining was foliation-parallel. Samples D600.1, D600.2, and D600.3 are from same run made at progressively greater distances from drain. Samples U3a and U3b are separate charges loaded in same run.

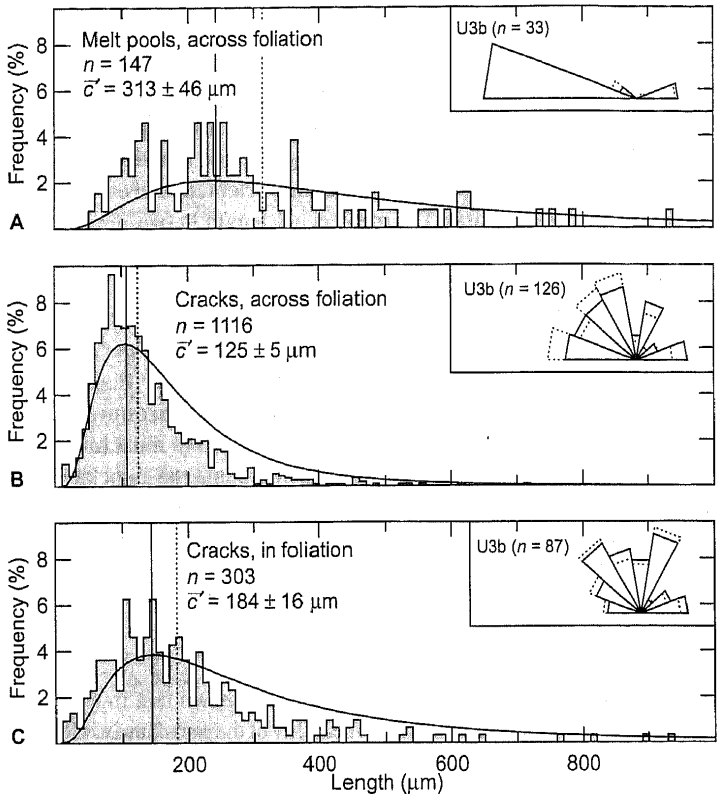

Figure 2. Length and orientation (rose diagrams) histograms. A: Long axis of melt pools orthogonal to foliation. B: Cracks orthogonal to foliation. C: Cracks in foliation plane. Length distributions are skewed relative to both lognormal (solid curve) and normal distributions (not shown), vertical lines locate means if lognormal (solid) and normal (dashed) populations are assumed. Uncertainties in our analysis are such that discrepancy between these means is insignificant; for simplicity we assume normal distributions. Number of observations = n. In rose diagrams (insets), dashed curves are the angular distribution weighted by length. These show that there is no significant tendency for cracks to be longer in any particular orientation.

(based on nine electron microprobe analyses), similar to the compositions reported by Brearley and Rubie (1990) for their water-saturated melting experiments. Assuming that the compositions of biotite and mullite in the present experiments are the same as those measured by Brearley and Rubie, the stoichiometry [balanced with respect to Si, Al, (K + Na), and (Mg + Fe)] of the melting reaction is

$$\text{muscovite} + 3.94\ \text{quartz} = 8.23\ \text{melt} + 0.03\ \text{biotite} + 0.16\ \text{mullite} \quad (1)$$

where the molar unit of each phase is defined on the basis of 22, 2, 2, 22, and 26 anion charges, respectively. If the phyllosilicates are fully hydroxylated, the melt composition required by equation 1 is

$$K_{0.0783}Na_{0.0310}Fe_{0.0053}Mg_{0.0110}Si_{0.8175}Al_{0.1902}O_{1.8822}(OH)_{0.2357}.$$

The molar volumes estimated for muscovite, quartz, melt, biotite, and mullite are, respectively, 140.8 , 22.7, 30.12, 149.6, and 134.6 cm^3/mol (Holland and Powell, 1990; Burnham, 1979; Bottinga et al., 1982); from these values, the volume change for the melting reaction is 44 cm^3 per mol of muscovite. As the initial rock contains 0.49×10^{-3} mol muscovite per cm^3, a dilational strain of 2.1% is required to accommodate melt production if the melt is not drained. In all undrained experiments the extent of reaction is >80% (Table 1); thus, the amount of dilational strain in each run was similar. The melt-filled crack propagating from the melt pool formed after muscovite is a physical expression of this strain (Fig. 1A). Toward intersections with melt pools, the cracks widen as a result of assimilation of the surrounding quartz. This observation, in combination with gravitational settling of mullite and biotite into the cracks, shows that the melt-filled cracks formed before the run was quenched.

Cracks that are orthogonal to the foliation commonly originate either from the tips of, and subparallel to, the melt pools or perpendicular to the long axis of melt pools (Fig. 1A). The former mode is not surprising in that the elliptical geometry of the melt pools should concentrate stress at their tips. Such

cracks often propagate preferentially in the direction of proximal melt pools, presumably because of interaction of the stress fields generated about adjacent pools. This process should enhance melt connectivity within the rock matrix.

The length of individual cracks is comparable to the grain size and varies little with experimental conditions, but does vary with sample orientation (Table 1). Consequently, the results of all experiments have been combined in the histograms B and C of Figure 2. The greater length of the cracks in the foliation plane (185 ± 8 μm), compared to those measured across the foliation (116 ± 6 μm), is probably related to the greater spacing of the melting sites in the foliation plane. Crack widths in two-dimensional section are typically about 4 μm, but because there is variation in crack thickness and the three-dimensional crack orientation is unknown, the true crack thickness cannot be more accurately constrained.

Total crack length per unit area (d) varies from 1000 to 4000 m/m^2 (Table 1), but is similar in sections taken from the same experimental charge, suggesting that the size of the images used for counting is statistically representative. Variation in total crack length in different experiments is not correlated with any experimental parameter. Since the strain represented by the cracks is proportional to the product of crack width and total length in two-dimensional section, variation in total length must be attributed to variation in crack width. If the strain represented by the cracks is equated to the volume change for the reaction, then the range of total crack length implies that average crack width is between 1 and 4 μm, which is comparable to the observed widths. The texture of the melt along the crack surface, as observed where grains have been plucked from the sample (Fig. 1B), indicates limited crack healing and textural equilibration on the time scale of the experiments (cf. Brantley, 1992).

The cracks have random orientation orthogonal to the foliation (Fig. 2B). In the plane of the foliation, some samples show a preferred crack orientation, but other samples do not (Fig. 2C). This variation is most probably related to the area of the individual muscovite grains, which is substantially larger in foliation-parallel sections. Consequently, the sample size for these sections may be too small to permit us to assess orientations reliably. The cracks exploit grain boundaries or cut individual grains with comparable frequency, which suggests that the grain boundaries have substantial strength. In all experiments made with a sand trap, the trap is completely saturated with melt, and there is no evidence of melt flow along the capsule-sample interface. Thus these experiments demonstrate that the microcracks form a permeable network. Images made at 2 mm intervals along the long axis of the core from run D600 (Table 1) show that total crack length per unit area decreases toward the sand trap. This decrease is consistent with collapse of the crack network due to drainage of the melt phase.

CRACK PERMEABILITY

The experimental results establish that the reaction-generated microcracks form a connected network but do not permit direct estimation of the permeability. To address this problem, we have used the statistical model of Dienes (1982) for the permeability of a network of randomly oriented penny-shaped cracks. That a model for randomly oriented penny-shaped cracks is appropriate can be argued from the general lack of preferred orientation and the similarity of crack lengths in sections both orthogonal and parallel to the rock foliation. In Dienes's model the key parameter related to connectivity is the probability, p, that an individual crack intersects one of its neighbors; this probability is expressed as

$$p = 1 - \exp\left[\frac{-\pi}{32} N \overline{c^3}\right], \tag{2}$$

where N is the crack density and c is the diameter of the penny-shaped cracks. There is no continuously connected pathway through a crack network if $p < 1/3$ (i.e., the percolation threshold), and the network is impermeable. For $p > 1/3$ a network of cracks, of aperture a, has a finite permeability that increases to

$$k = \frac{\pi N \overline{a^3 c^2}}{15} \tag{3}$$

at $p = 1$, when the cracks form a fully connected network. In equations 2 and 3, the high-order moments can be approximated by powers of the mean, provided the distribution of the property is relatively narrow (e.g., $\overline{c^2} \approx \overline{c}^2$). If the observed cracks are the traces of disklike cracks in three dimensions, then the diameter of the disks is $\sim 3/2\ \overline{c}'$, where $\overline{c}'$ is the two-dimensional average length (Thompson, 1972). If the cracks are approximated by two-dimensional disks, the total area of the cracks per unit volume of rock is identical to the total length of cracks exposed in any two-dimensional section of unit area (d, Table 1) multiplied by a unit length ($\hat{l}$). The crack density is then $N \approx (16 d\hat{l})/(9\pi \overline{c}'^2)$. From equation 2, the inferred crack densities ($N = 10^{10}$ to 10^{11} m^{-3} for $\overline{c}' = 151$ μm) and lengths are inadequate to affect connectivity (i.e., $p = 0.03$–0.11), but the melt pools compose a second set of hydraulic bonds. If the preferred orientation of the melt pools is discounted (an assumption that may be justified by the relatively small number of melt pools) and the two populations of hydraulic bonds ($d_{\text{melt pool}} = 2948$ m^{-1}, $\overline{c}'_{\text{melt pool}} = 313$ μm) combined, then Dienes's model yields $p = 0.4$–0.5, which is above the percolation threshold, consistent with our experimental evidence for connectivity. As it is unlikely that the melt pools affect connectivity by themselves, the permeability of the combined melt pool-crack network is most likely limited by the permeability of the cracks (cf. Faul, 1997). The functional dependence of the permeability for $1/3 < p < 1$ is difficult to assess, but initially rises as the square of p. Given this relation, it seems reasonable to approximate the permeability of the complete network by equation 2 and by using the properties of the cracks alone. The permeabilities we obtain in this manner are 10^{-13}–10^{-15} m^2 ($a = 1$–4 μm). Such permeabilities are at least four orders of magnitude greater than those characteristic of regional metamorphic environments (e.g., Yardley, 1986). Moreover, if our assumptions are tenable, this permeability is isotropic, in contrast to that in texturally equilibrated systems, where rock fabric leads to highly anisotropic permeability (Laporte and Watson, 1995).

DISCUSSION

Our results show that relatively small dilational strains are capable of generating permeable microcrack networks. For such a mechanism to be viable in natural environments, the dilational strain rate required for the reaction to progress must be greater than the rate at which porosity can be created by plastic deformation (creep). Because the dilational strain rate by creep is proportional to the porosity (Wilkinson and Ashby, 1975), the critical condition determining whether the deformation is brittle or plastic occurs at the onset of the reaction when the porosity (melt-filled) is low and poorly connected. Under these conditions melt-enhanced diffusion creep is unimportant (Dell'Angelo et al. 1987), and dislocation creep is the most probable mechanism of plastic deformation. Wilkinson and Ashby (1975) have given the rate of porosity production by dislocation creep as

$$\frac{d\phi'}{dt} = -D f_{H_2O} \exp\left(\frac{-Q}{RT}\right)\left(\frac{3}{4}\right)^{n+1} \frac{\phi}{\left(1-\phi^{1/n}\right)^n}\left(\frac{P_e}{n}\right)^n \tag{4}$$

where P_e is the effective pressure (confining pressure–fluid pressure), T is the temperature, ϕ' is the porosity generated by strain, is the absolute porosity, R is the gas constant, f_{H_2O} is the water fugacity, and n, D, and Q are empirical constants in the Dorn equation used to relate the strain rate of the material to an applied flow stress (e.g., Kohlstedt et al., 1996). If an anatectic reaction front of width w advances at velocity v, then the average porosity production in excess of that created by the reduction in solid volume is

$$\frac{d\phi'}{dt} = \frac{v}{w}\Delta V \tag{5}$$

where ΔV is the volume change of the reaction per unit volume of rock and v/w is the reaction rate. Creep will be most effective when $-P_e$ is just below the tensile strength of the rock (6–50 MPa, e.g., Guegen and Palciauskas, 1994). Equating equations 4 and 5 at this condition gives the minimum width of the reaction front necessary for reaction-induced deformation to be accommodated by creep, as plotted in Figure 3 as a function of the reaction front velocity and temperature. During regional metamorphism, isotherms,

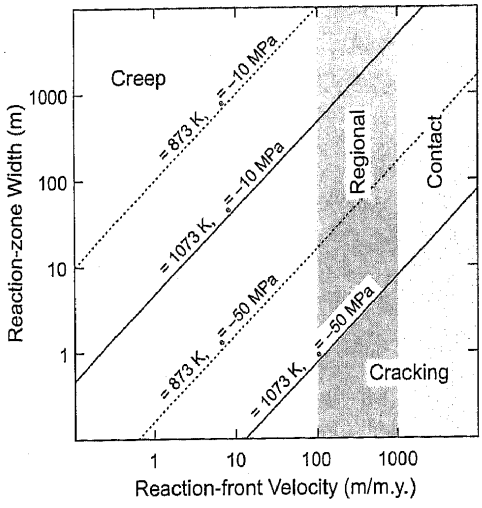

Figure 3. Minimum reaction-zone width at which reaction-induced dilational strain can be accommodated by creep as function of reaction front velocity, temperature (T), and the effective pressure (P_e) at which cracking occurs. Cracking occurs if reaction zone is narrower than this width. Computed from equations 3 and 4 for water-saturated quartzite ($D = 1.8 \times 10^{-11}$ MPa^{-3}, $n = 4$, $Q = 150$ kJ/mol; after Luan and Paterson, 1992), an initial porosity of 0.1%, and $\Delta V = 2.1\%$. During regional metamorphism, reaction fronts propagate at ca. 100–1000 m/m.y.; higher rates can be attained during regional contact metamorphism.

and therefore metamorphic reaction fronts, typically advance at 100 to 1000 m/m.y. (e.g., Rubie, 1986; Thompson, 1989), and univariant reaction fronts are <100 m wide (e.g., Lasaga, 1986; Pattison, 1992). For these parameters (Fig. 3), deformation would be brittle if the tensile strength of the rock was near the lower limit of measured values for crystalline rocks and the initial porosity was <0.1%. Substantially higher heating rates may be achieved during regional contact metamorphism. Thus we conclude that reaction-generated microcracking is a plausible, but not inevitable, mechanism for enhancing the permeability of anatectic systems. The dilational strain generated by many metamorphic devolatilization reactions is comparable to that of the melting reaction studied here, and rocks with power-law-creep rheologies become stronger with decreasing temperature. Consequently, reaction-induced microcracking may also be important during devolatilization, which is otherwise analogous to partial melting.

In the foregoing analysis we neglect the effect of drainage on fluid pressure and reaction kinetics (Connolly, 1997) and the effect of crack healing. Given the extremely low permeabilities ($<10^{-20}$ m^2) required to maintain elevated fluid pressures on a metamorphic time scale (e.g., Yardley, 1986), the permeability of the unreacted rocks overlying a zone of crustal anatexis may be such that drainage by pervasive flow is insignificant until a more efficient mechanism for melt extraction develops (cf., Clemens and Mawer, 1992; Petford, 1995). Reaction-induced microcracking may increase the efficiency of this process, by increasing the permeability within partially melted rocks. The time scale of our experiments is such that crack healing (Fig. 2B) does not limit connectivity, but in natural environments the competition between crack generation and healing may be more important. If crack healing is rapid enough, then reaction-induced microcracking alone will be incapable of creating a permeable crack network. Even in such a scenario, reaction-induced microcracking may play an important role in melt extraction if the cracks are kept open or augmented by externally driven deformation.

ACKNOWLEDGMENTS

This project would not have been possible without financial support from ETH-Forschungsprojekt 0-20-885-94 and the support of the Natural Environment Research Council (UK) for the high P-T experimental facilities at Edinburgh. We thank Tom Blenkinsop, Nicholas Petford, and Brooks Hanson for critical reviews; Djordje Grujic, Karsten Kunze, Rolf Schmid, and Marcel Pfiffner for assistance with imaging techniques; Ernie Rutter for providing the sand used in our experiments; and Dave Olgaard for an explanation of deformation.

REFERENCES CITED

Bottinga, Y., Weill, D., and Richet, P., 1982, Density calculations for silicate liquids. I. Revised method for aluminosilicate compositions: Geochimica et Cosmochimica Acta, v. 46, p. 909–919.

Brantley, S. L., 1992, The effect of fluid chemistry on quartz microcrack lifetimes: Earth and Planetary Science Letters, v. 113, p. 145–156.

Brearley, A. J., and Rubie D. C., 1990, Effects of H_2O on the disequilibrium breakdown of muscovite + quartz: Journal of Petrology, v. 31, p. 925–956.

Burnham, C. W., 1979, Magmas and hydrothermal fluids, *in* Barnes, H. L., ed., Geochemistry of hydrothermal ore deposits: New York, Wiley, p. 71–136.

Clemens, J. C., and Mawer C. K., 1992, Granitic magma transport by fracture propagation: Tectonophysics, v. 204, p. 339–360.

Connolly, J. A. D., 1997, Devolatilization-generated fluid pressure and deformation-propagated fluid flow during prograde regional metamorphism: Journal of Geophysical Research (in press).

Dell'Angelo, L. N., Tullis, J., and Yund, R. A., 1987, Transition from dislocation creep to melt-enhanced diffusion creep in fine-grained granitic aggregates: Tectonophysics, v. 139, p. 325–332.

Dienes, J. K., 1982, Permeability, percolation and statistical crack mechanics, *in* Goodman, R. E., and Heuze, F. E., eds., Issues in rock mechanics: New York, American Institute of Mineralogical, Metallurgical and Petroleum Engineering, p. 86–94.

Faul, U. H., 1997, The permeability of partially molten upper mantle rocks from experiments and percolation theory: Journal of Geophysical Research (in press).

Grapes, R. H., 1986, Melting and thermal reconstitution of pelitic xenoliths, Wehr Volcano, East Eiffel, Germany: Journal of Petrology, v. 27, p. 343–396.

Guegen, Y., and Palciauskas, V. V., 1994, Introduction to the physics of rocks: Princeton, New Jersey, Princeton University Press, 294 p.

Holland, T. J. B., and Powell, R., 1990, An enlarged and updated internally consistent dataset with uncertainties and correlations: Journal of Metamorphic Geology, v. 8, p. 89–124.

Laporte D., and Watson E. B., 1995, Experimental and theoretical constraints on melt distribution in crustal sources: Implications for the segregation of granitic magmas: Chemical Geology, v. 124, p. 161–184.

Lasaga, A. C., 1986, Metamorphic reaction rate laws and development of isograds: Mineralogical Magazine, v. 50, p. 359–373.

Luan, F. C., and Paterson, M. S., 1992, Preparation and deformation of synthetic aggregates of quartz: Journal of Geophysical Research, v. 97, p. 301–320.

Kohlstedt, D. L., Evans, B., and Mackwell, S. J., 1996, Strength of the lithosphere: Constraints imposed by laboratory experiments: Journal of Geophysical Research, v. 100, p. 17587–17602.

McKenzie, D. P., 1985, The extraction of magma from the crust and mantle: Earth and Planetary Science Letters, v. 74, p. 81–91.

Miller, C. F., Watson, E. B., and Harrison, T. M., 1988, Perspectives on the source segregation and transport of granitoid magmas: Royal Society of Edinburgh Transactions, Earth Sciences, v. 79, p. 139–156.

Moecher, D. P., O'Hara, K. D., Sharp, Z. D., and Allen, J. L., 1996, O isotope systematics of pseudotachylite and gneissic wall rock from the Homestake shear zone, central Colorado: Geological Society of America Abstracts with Programs, v. 28, no. 7, p. A-382.

Pattison, D. R. M., 1992, Stability of andalusite and sillimanite and the Al_2SiO_5 triple point constraints from the Ballachulish aureole, Scotland: Journal of Geology, v. 100, p. 423–446.

Petford, N., 1995, Segregation of tonalitic-trondhjemitic melts in the continental crust: The mantle connection: Journal of Geophysical Research, v. 100, p. 15735–15743.

Rubie, D. C., 1986, The catalysis of mineral reactions by water and restrictions on the presence of aqueous fluid during metamorphism: Mineralogical Magazine, v. 50, p. 399–415.

Rutter, E. H., and Neumann, D. H. K., 1995, Experimental deformation of partially molten westerly granite under fluid-absent conditions, with implications for the extraction of granitic magmas: Journal of Geophysical Research, v. 100, p. 15697–15715.

Serra, J., 1988, Image analysis and mathematical morphology: Theoretical advances: London, Academic Press, 411 p.

Storre, B., 1972, Dry melting of muscovite + quartz in the range $P = 7$ kb to $P = 3$ kb: Contributions to Mineralogy and Petrology, v. 37, p. 87–89.

Thompson, A. W., 1972, Calculation of true volume grain diameter: Metallography, v. 5, p. 366–369.

Thompson, P. H., 1989, Moderate overthickening of thinned sialic crust and the origin of granitic magmatism and regional metamorphism in low-P-high-T terranes: Geology, v. 17, p. 520–523.

Wilkinson, D. S., and Ashby, M. F., 1975, Pressure sintering by power law creep: Acta Metallurgica, v. 23, p. 1277–1285.

Wolf, M. B., and Wyllie, P. J., 1991, Dehydration melting of solid amphibolite at 10 kbar: Textural development, liquid interconnectivity and applications to the segregation of magmas: Contributions to Mineralogy and Petrology, v. 44, p. 151–179.

Yardley, B. W. D., 1986, Fluid migration and veining in the Connemara Schists, Ireland, *in* Walther, J. V., and Wood, B. J., eds., Fluid-rock interactions during metamorphism: New York, Springer-Verlag, p. 89–108.

Manuscript received December 23, 1996
Revised manuscript received April 9, 1997
Manuscript accepted April 19, 1997